Meteoritics & Planetary Science 39, Nr 7, 1187–1197 (2004)
Abstract available online at http://meteoritics.org

Fluid inclusion evidence for impact-related hydrothermal fluid and hydrocarbon migration in Creataceous sediments of the ICDP-Chicxulub drill core Yax-1

Volker LÜDERS[1*] and Karen RICKERS[1, 2]

[1]GeoForschungsZentrum Potsdam, Department 4, Telegrafenberg, D-14473, Potsdam, Germany
[2]Hamburger Synchrotronstrahlungslabor HASYLAB at Deutsches Elektronen-Synchrotron DESY, Notkestrasse 85, D-22603 Hamburg, Germany
*Corresponding author. E-mail: volue@gfz-potsdam.de

(Received 3 September 2003; revision accepted 31 March 2004)

Abstract–Fluid inclusions studies in quartz and calcite in samples from the ICDP-Chicxulub drill core Yaxcopoil-1 (Yax-1) have revealed compelling evidence for impact-induced hydrothermal alteration. Fluid circulation through the melt breccia and the underlying sedimentary rocks was not homogeneous in time and space. The formation of euhedral quartz crystals in vugs hosted by Cretaceous limestones is related to the migration of hot (>200 °C), highly saline, metal-rich, hydrocarbon-bearing brines. Hydrocarbons present in some inclusions in quartz are assumed to derive from cracking of pre-impact organic matter. The center of the crater is assumed to be the source of the hot quartz-forming brines. Fluid inclusions in abundant newly-formed calcite indicate lower cyrstallization temperatures (75–100 °C). Calcite crystallization is likely related to a later stage of hydrothermal alteration. Calcite precipitated from saline fluids, most probably from formation water. Carbon and oxygen isotope compositions and REE distributions in calcites and carbonate host rocks suggest that the calcite-forming fluids have achieved close equilibrium conditions with the Cretaceous limestones. The precipitation of calcite may be related to the convection of local pore fluids, possibly triggered by impact-induced conductive heating of the sediments.

INTRODUCTION

Meteoritic impacts are believed to cause hydrothermal fluid circulation in the crater fill and surrounding rocks due to the release of large amounts of thermal energy (Dence at al. 1977). Heat sources for impact-generated hydrothermal systems include conductive cooling from the central uplift (Crossey et al. 1994), inherent heat in the impact process (Dence et al. 1977), and cooling of the melt sheet through convection (Ames et al. 1998). Impact-induced hydrothermal activity has been suggested for several impact sites. At the marine Lockne impact structure, Sweden, seawater rushed back into the crater forming a hydrothermal system initiated by the residual heat in the structure, which let to the precipitation of (mainly) calcite in cavities and fractures (Sturkell 1998). At the Ilyinets crater, Ukraine, the impact breccias are strongly altered and have elevated potassium contents but lower sodium contents than the target rocks, probably due to the alteration by an impact-induced hydrothermal system (Gurov et al. 1998). K-metasomatism was observed in the impactites of the Chicxulub drill core Yaxcopoil-1 (Yax-1) (Hecht et al. 2003). U-Pb geochronological data have revealed evidence that the formation of hydrothermal Zn-Pb-Cu deposits (6 Mt) at the top of the suevite in the crater fill at the 1.85 Ga terrestrial Sudbury structure was related to an impact-generated hydrothermal system (Ames et al. 1998). Osinski et al. (2001) attributed different hydrothermal mineral assemblages hosted in cavities and fracture fillings in polymict breccias and pipes to three distinct stage of alteration within the Haughton impact structure, Canada. The paragenetic sequence is early quartz from vapor-dominated fluids above 200 °C, followed by the main stage characterized by the precipitation of calcite, sulfates, fluorite, and marcasite at 200–100 °C, and finally, selenite and fibro ferrite precipitated below 100 °C near the base of the breccia sheet.

Fluid inclusions trapped in newly-formed minerals or trails of secondary inclusions in pre-existing mineral phases can also provide information for impact-related hydrothermal activity as shown by fluid inclusion studies at several impact localities (e.g., Stöffler at al. 1977; Komor et al. 1988; Koeberl et al. 1989; Boer et al. 1996; Sturkell et al. 1998; Molnar et al. 1999, 2001; Kirsimae et al. 2002).

The formation of the Chicxulub impact crater is likely related to meteoritic impact at the Cretaceous-Tertiary

boundary 65 Ma ago (e.g., Alvarez et al. 1980; Hildebrand et al. 1991; Pope et al. 1991, 1996; Krogh et al. 1993; Morgan et al. 2000; Dressler et al. 2003). Anhydrite-hosted fluid inclusions from the drill hole Y-6 in the Chicxulub impact crater, Yucatán, Mexico have been studied by Gonzales-Partida et al. (2000). The fluid inclusions are characterized by heterogeneous phase assemblages within the same crystal planes (i.e., coexisting liquid + vapor, vapor-rich, and liquid + vapor + solid inclusions). Calculated salinities derived from final ice melting temperatures and dissolution temperatures of halite daughter minerals range between 3.6 and 23 wt% NaCl equivalent for liquid + vapor inclusions and between 36 and 42 wt% NaCl equivalent for liquid + vapor + halite inclusions. Measured homogenization temperatures ranged between 100 and 500 °C. The data are interpreted to represent a cooling trend with late boiling due to the ejection of hot impact breccia into an aqueous medium (Gonzales-Partida et al. 2000).

Zürcher et al. (2003) estimated formation temperatures of about 300 ± 40 °C for vein calcites on the basis of carbon and oxygen isotopic compositions, assuming a Cretaceous seawater source for the mineral forming fluids.

This paper focuses on samples collected from the ICDP-Chicxulub drill core Yax-1 that penetrated 600 m of Cretaceous carbonates and evaporates (sulfates) that underlie a unit of impactites (Dressler et al. 2003). Open-space fillings with euhedral calcite crystals up to 1 cm in size are abundant within the massive Cretaceous limestone and in the suevitic breccia. Two fractures filled with quartz were found about 100 m below the suevitic breccia (Table 1). One of the quartz samples also contains calcite that is grown on quartz (Fig. 1). The interval between 1300 and 1510 m contains numerous layers that are rich in organic matter.

Our study aims at tracing post impact alteration processes in secondary minerals in the Yax-1 drill core on the basis of detailed fluid inclusion studies, REE distribution, and stable isotope geochemistry.

SAMPLE DESCRIPTION

Coarse recrystallized calcites in vugs were collected from the monomict melt breccia (Table 1). Two generations of calcite were identified in most of the samples: 1) an early milky calcite and 2) a late clear calcite generation that replaces or overgrows the first generation calcite. Euhedral yellow or white calcite crystals were collected from vugs hosted by Cretaceous limestone or calcarenite (Table 1). Beds of recrystallized dolomite rhombohedrons associated with small crystals of pyrite within limestone were found in a sample at 1348.58 m depth (Fig. 4a).

For comparison, a calcite-filled vug within Tertiary limestone was sampled (Table 1).

Quartz-filled fractures were found within brecciated calcarenitic host rocks at 990.23 m, 990.3 m, and 1000.53 m, respectively. The aggregates of clear euhedral quartz crystals are 1–5 mm long. The center of the quartz vug at 990.23 m is filled with calcite indicating that quartz precipitation occurred prior to the crystallization of calcite (Fig. 1).

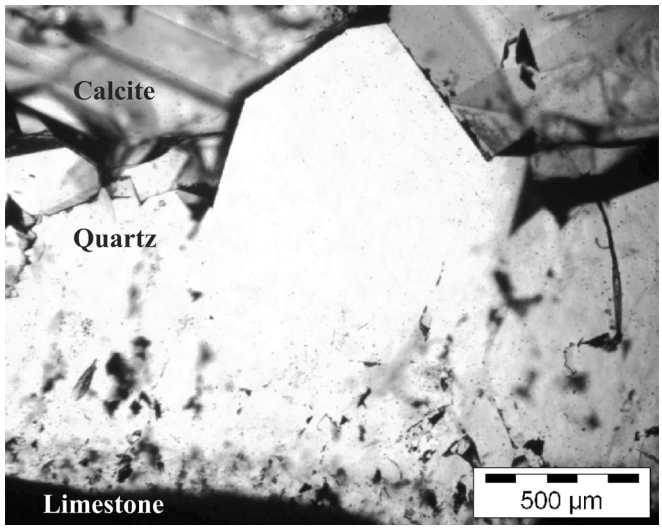

Fig. 1. Microphotograph showing quartz crystals grown on limestone. The quartz crystals are overgrown by younger calcite (Yax-1_990.23 m).

Secondary anhydrite was collected from interlayered anhydrite in calcarenite and dolomite units in the depth interval of 1323.87 m to 1399.05 m.

Black and dark brownish layers up to 1 cm wide as well as dark coatings around anhydrite nodules are enriched in organic matter. The fine-grained mineral assemblage consists of K-feldspar, dolomite, pyrite, marcasite, and apatite set in a dense organic-rich groundmass. Thicker organic-rich layers display ductile flow features indicated by foliation, aligned and stretched minerals, and rounded porphyroclasts. The organic-rich layers are displaced by brittle shear zones and are offset by clastic dike breccias (Kenkmann et al. 2003). This indicates that kerogen-rich layers existed before the dikes formed, and thus, prior to the impact. Remobilization of bitumen and oil occurred after the emplacement of the dikes and may have been accelerated by an impact-induced thermal overprint. Brittle shear zones and dikes were used as pathways and hosts. Seven samples from the interval of 1398–1461 m (Table 1) contain total organic carbon between 0.06 and 0.66 wt% for fine grained carbonates, and 0.75–6.77 wt% in darker, stained zones (Lüders et al. 2003).

ANALYTICAL PROCEDURE

Conventional Microthermometry

Microthermometric measurements were conducted using a USGS heating/freezing system mounted on a BX50

Table 1. Summary of sample origin, lithological units (after Dressler et al. 2003), oxygen and carbon isotope compositions, and ranges of salinity and homogenization temperatures of fluid inclusions.

Sample #	Depth (m)	Unit	Sample material	$\delta^{18}O$ (‰ VSMOW)	$\delta^{13}C$ (‰ PDB)	Salinity (wt% eq. NaCl)	Range of Th (°)
1830	444.4	Tertiary	Limestone	28.2	0.54	–	–
1830	444.4	Tertiary	Calcite (vug)	–1.19	25.1	–	–
1835	866.63	Monomict melt breccia	Calcite (vug)	–	–	–	74.2–111 (5)
1837	875.6	Monomict melt breccia	Limestone	23.3	–0.02	–	74.9 (1)
1837	875.6	Monomict melt breccia	Calcite (vug)	23.9	–0.71	–	–
1839	888.17	Monomict melt breccia	Calcite (vug)	23.1	1.91	–	–
1801	896.68	Limestone	Limestone	22.8	1.86	–	–
1801	896.68	Limestone	Calcite (vug)	23.4	2.21	–	–
1836	897.05	Limestone	Limestone	23.4	1.97	–	–
1836	897.05	Limestone	Calcite (vug)	23.4	2.20	–	73.3–103.8 (5)
2127	990.23	Limestone	Quartz/Calcite (vug)	–	–	16.1–32 (8)	235.6–278.2 (7)
1824	990.3	Calcarenite	Quartz (vug)	–	–	14.1–37 (14)	220.2–285 (9)
1819	1000.53	Calcarenite	Quartz (vug)	–	–	15–16.3 (12)	120.9–193.9 (8)
1819	1000.53	Calcarenite	Limestone	23.0	2.90	–	–
1819	1000.53	Calcarenite	Limestone	22.7	2.07	–	–
1803	1005.27	Calcarenite	Limestone	24.1	–0.01	–	–
1803	1005.27	Calcarenite	Calcite (vug)	23.1	0.96	–	–
1807	1085.44	Calcarenite/Anhydrite	Organic matter	–	–	–	–
1820	1132.16	Calcarenite/Anhydrite	Organic matter	–	–	–	–
1348.36	1348.36	Calcarenite	Dolomite (recryst.)	–	–	7.5–7.9 (5)	65.1–96.8 (9)
1813	1398.35	Calcarenite	Organic matter	–	–	–	–
1810	1411.45	Calcarenite	Organic matter	–	–	–	–
1811	1418.8	Calcarenite	Organic matter	–	–	–	–
1816	1435.37	Dolomite/Anhydrite	Organic matter	–	–	–	–
1817	1436.04	Dolomite/Anhydrite	Organic matter	–	–	–	–
1815	1451.39	Dolomite/Anhydrite	Organic matter	–	–	–	–
1818	1453.08	Calcarenite	Organic matter	–	–	–	–
1814	1461.17	Calcarenite	Organic matter	–	–	–	–

Olympus microscope. The stage was calibrated with synthetic inclusions supplied by Synflinc.

Laser Raman Spectroscopy

Hydrocarbon-bearing fluid inclusions hosted in quartz were analyzed with a Jobin-Yvon (formerly Dilor) Raman spectrometer (model LabRam). The exciting radiation used was a 532 nm Nd/Yag laser.

Stable Isotope Mass Spectrometry

Carbon and oxygen isotopes were measured online using a Finnigan DELTAplusXL mass spectrometer in combination with a Gasbench II. The carbonates were finely grounded and 0.25 mg of sample powder was reacted with 100% phosphoric acid at 72 °C to liberate CO_2. The accuracy of the measurement is greater than 0.1 ‰. All samples are referred to the NBS 19 standard. Carbon isotope ratios are reported relative to PDB (Peedee belemite), standard and oxygen isotope ratios are reported relative to V-SMOW (Standard Vienna Mean Ocean Water). Isotopic data are reported in δ notation, $\delta = [(R_{sample}/R_{standard})] - 1 \times 1000$, where R = either $^{13}C/^{12}C$ or $^{18}O/^{16}O$.

ICP-MS Analysis

Sub-samples of calcite and host rock were finely ground in an agate mortar. The analytical procedure is described in detail elsewhere (Dulski 2001). About 0.05 g of sample powder was dissolved in 6 M HNO_3. Before analysis, Ru and Re were added to aliquots of the solutions as internal standards for drift correction, and the mixtures were diluted by a factor of 10 or 2, depending on the REE concentration of the specific sample. Solutions prepared following the above procedure show a dilution factor of 2500 to 4000 and are about 0.5 mol l^{-1} in HNO_3. ICP-MS measurements have been performed using an ELAN 5000A quadrupole ICP mass spectrometer (Perkin-Elmer/SCIEX, Canada).

Synchrotron X-Ray Fluorescence Analysis

Single fluid inclusion analyses have been performed at the SR XRF microprobe at beamline L (Lechtenberg et al. 1996) at the Hamburger Synchrotronstrahlungslabor (HASYLAB) at Deutsches Elektronen Synchrotron DESY, Hamburg, Germany. For our measurements, we used the polychromatic X-ray continuum of a bending magnet of

DORIS III (maximum brilliance at 16.6 keV) filtered by a 1 mm Al absorber increasing peak to background ratios of the low energy part of the spectra. The resulting X-ray spectral distribution allows simultaneous major and trace element analysis of elements with Z between 19 and 82 via K-shell excitation.

The incoming beam was collimated with a cross-slit system and, additionally, by a monocapillary with an inner diameter of 20 μm, resulting in a cross-section of the beam on the sample of 15 μm. The spectra were recorded in a nitrogen cooled energy-dispersive high-purity germanium detector (Gresham) at 90° to the incoming beam. This geometry guarantees optimal background reduction (Vincze et al. 1995a). The sample was oriented at 45° to the incoming beam and to the detector. A 2.2 mm diameter pinhole was placed at 10 mm in front of the detector window. The distance between the sample surface and the detector was 22 mm.

Fluid inclusions were measured in quartz matrix only. Samples were always double-polished thin sections with a maximum thickness of 200 μm. Area scans of 10 μm steps in each direction were performed over single inclusions. Sample times per point varied between 150 and 600 sec. Peak fitting and the calculation of peak areas was performed with the software package AXIL (Van Espen et al. 1992). Concentrations were retrieved in the standardless mode using Monte Carlo simulations (Vincze et al. 1993, 1995b, c) following the procedure described in detail in Rickers et al. (2004).

REE DISTRIBUTION AND $\delta^{18}O$ VERSUS $\delta^{13}C$ RELATIONSHIPS IN LIMESTONE AND CALCITES

The Tertiary limestone sample (444.4 m; Table 1) shows a shale-normalized ($_{SN}$) REE pattern that is slightly depleted in LREE and flat from the MREE to the HREE, except for a slight decrease from Er to Lu (Fig. 2). It exhibits a small positive Gd_{SN} anomaly and negative Ce_{SN} anomaly. Such a REE distribution is typical of aluminosilicate-free marine sedimentary carbonates and modern seawater (Bau and Dulski 1996; Webb and Kamber 2002). Remobilized calcite from a vug hosted by Tertiary limestone (444.4 m; Table 1) shows a REE distribution pattern similar to that of the surrounding host rock, except that the total REE content is lower (Table 2).

In contrast, the REE_{SN} distribution patterns of the Cretaceous limestone samples (NG samples in Fig. 2) decrease from La to Sm and are flat from the MREE to the HREE. They all show small positive Gd_{SN} anomalies, but no negative Ce_{SN} anomalies (Fig. 2). In cases where limestones bear clay minerals, the REE patterns are enriched in LREE and the Ce_{SN} anomaly disappears during recrystallization as a result of diagenesis (Möller et al. 2003). Recrystallization of Cretaceous limestone also caused a decrease in Sr content, which is lower by an order of magnitude when compared with the reference sample from the Tertiary unit (Table 2). The REE_{SN} patterns of calcites from vugs in Cretaceous limestone show similar trend as their host rocks, thus, indicating that they precipitated from fluids which had achieved close equilibrium with the limestones. These fluids either could have been formation waters or seawater that penetrated the marine detritus-rich limestone. In the latter case, long-term water-rock interaction under (nearly) closed-system conditions was necessary to equilibrate with the limestone. The absence of positive Eu anomalies in the REE_{SN} patterns of recrystallized calcites indicate that mineral precipitation did not occur from fluids that have experienced temperatures above 250 °C (Bau and Möller 1992) and exclude that the fluids were derived from extraneous sources at great depth or from high temperature formation waters heated by an enhanced thermal gradient.

Carbon and oxygen isotopic compositions were measured in samples from the Cretaceous sequence and calcites from fissures that were also analyzed for REE as described above. The oxygen and carbon isotopic compositions of host rocks and fissure calcites show only small isotopic variations (Table 1). The host rock samples show $\delta^{18}O$ values between 22.7 and 25.1‰ when normalized to V-SMOW and $\delta^{13}C$ values between –0.02 and 2.9‰ (PDB). These values are typical for diagenetic limestones (Veizer 1992). The $\delta^{13}C$ and $\delta^{18}O$ values of vein calcite are similar to those of the host rocks (Fig. 3). For individual samples, the variation in $\delta^{18}O$ and $\delta^{13}C$ between host rock and fissure calcite is 1‰ (maximum) for oxygen and 0.7‰ for carbon (Table 1). The $\delta^{13}C$ and $\delta^{18}O$ values of the analyzed calcites (Table 1) fall into the same range as the $\delta^{13}C$ and $\delta^{18}O$ values for vein calcites from the Yax-1 drill site reported by Zürcher et al. (2003). The observed small variations of the $\delta^{18}O$ and $\delta^{13}C$ values indicate the calcite-forming fluids were in close equilibrium with the host rocks rather than being derived from a large scale circulating hydrothermal system. The calcite-forming fluids did not interact with organic material in the Cretaceous limestones as this would result in lighter (more negative) $\delta^{13}C$ values. Therefore, it seems very likely that fissure calcites precipitated from local formation waters, which is also supported by the results of the REE studies.

The stable isotope signatures of calcites in Yax-1 drill core differ significantly from calcites analyzed in Y-6 located closer to the center of the crater (Kettrup et al. 2000). Variation in the mean $\delta^{13}C$ values is minor (about 3‰), however, the $\delta^{18}O$ variation is significant, up to 15‰ between the calcite samples from the drill cores Y-6 and Yax-1 (Fig. 3). Since oxygen isotopic fractionation increases with decreasing temperature in fluid-mineral systems (O'Neil et al. 1969; Clayton et al. 1972), the large fractionation of the $\delta^{18}O$ values may be indicative for higher crystallization temperatures of at least 100 °C (O'Neil et al. 1969; Clayton et al. 1972; Zheng 1994) for the calcites from the Y-6 drill core assuming a homogeneous fluid source (i.e., formation water).

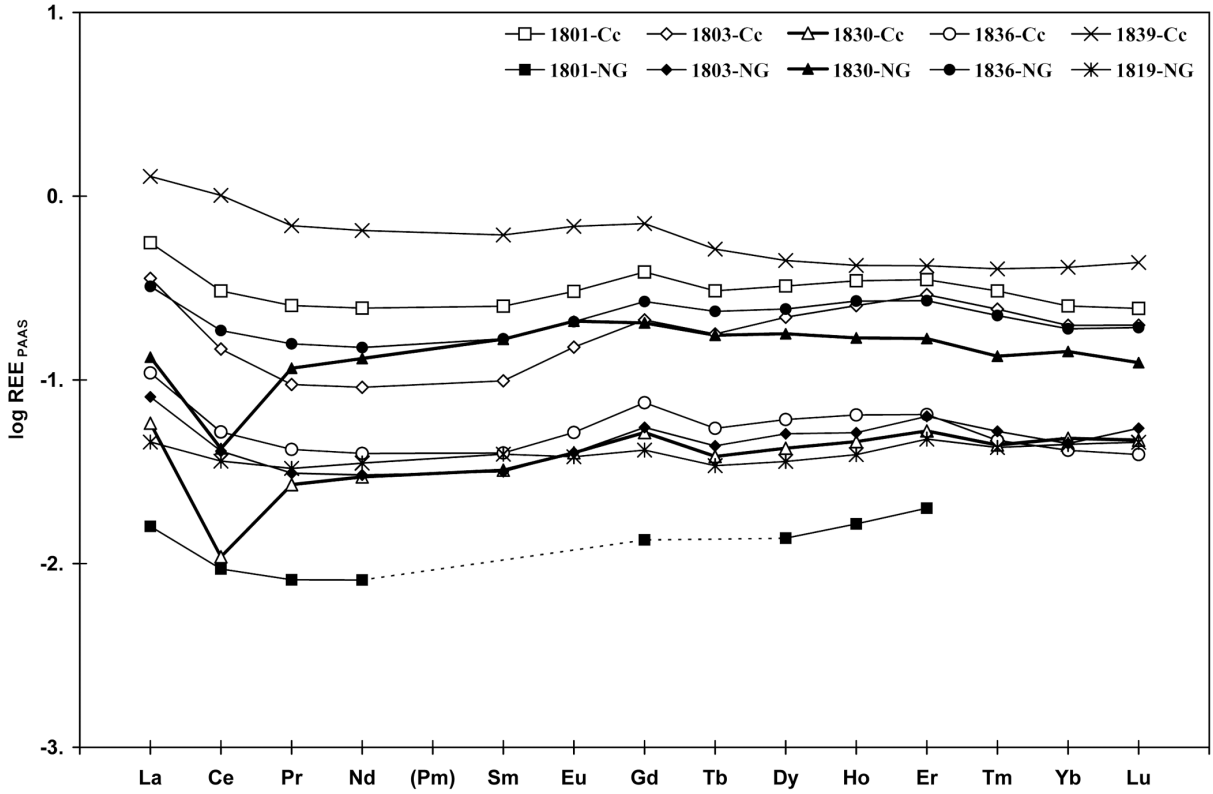

Fig. 2. PAAS-normalized REE distribution patterns of Tertiary (1830-NG) and Cretaceous limestone samples (1801-NG, 1803-NG, 1836-NG, 1819-NG) and calcites (1801-Cc, 1803-Cc, 1830-Cc, 1836-Cc, 1839-Cc) from vugs. The calcite sample 1830-Cc is hosted by Tertiary limestone, all other calcite samples originate from the Cretaceous megablock (for sample origin, see Table 1).

FLUID INCLUSION STUDIES

Fluid Inclusion Petrography

Recrystallized anhydrite from the Yax-1 drill core contain monophase aqueous inclusions in contrast to that reported for samples from the Y-6 drill core (Gonzales-Partida et al. 2000). Monophase aqueous inclusions in anhydrite are mostly very small <5 μm and show rectangular shapes. They are orientated parallel to the {101} or {001} crystal planes and are classified to be of primary origin (Roedder 1984).

Primary fluid inclusions in sparry calcite from the suevitic breccia and in calcite crystals from vugs are rarely found. When present, these fluid inclusions mostly occur in growth zones adjacent to rock fragments. Two-phase inclusions show irregular, elongated or rounded forms and sizes up to 30 μm. Vapor bubbles occupy not more than 3–5% by volume of the inclusions (Fig. 4b). Leakage of primary inclusions shown by highly variable liquid/vapor ratios was observed in sparry calcite from the suevitic breccia. Fluid inclusions in clear recrystallized calcite are always monophase aqueous and of secondary origin. They occur in clusters decorating crystal planes or are arranged along trails crosscutting through calcite. They have either rounded-elongated or irregular forms (Fig. 4c). The sizes of secondary fluid inclusions in calcite seldom exceed 10 μm.

Recrystallized carbonate lenses and fractures within massive limestone also host primary two-phase (Fig. 4b) or secondary monophase fluid inclusions similar in shape and size to those described in calcite from the suevitic breccia.

Quartz crystals in vugs within Cretaceous limestones (samples 1819, 1824, and 2127 in Table 1) host a different type of primary fluid inclusions when compared with calcite. Three compositional types of fluid inclusions can be distinguished: 1) two-phase aqueous fluid inclusions (Fig. 4d); 2) two-phase aqueous fluid inclusions hosting a cubic (most probable halite) daughter mineral (Fig. 4e); and 3) polyphase fluid inclusions with a small aqueous phase, a dark vapor bubble and at least one solid phase (Fig. 4f). Primary fluid inclusions in quartz always occur at the base of the quartz crystals and are often orientated parallel to growth zones (Fig. 4f). The size of quartz-hosted fluid inclusions varies between 10 to 50 μm. For unknown reason, many of the inclusions show very inconsistent liquid/vapor ratios. In the upper parts of the quartz crystals only single phase aqueous inclusions were found. Thus, indicating that the crystallization temperature must have dropped very rapidly during crystal growth. Calcite overgrowing quartz in sample Yax-1_990.23 m (Fig. 1) also hosts single phase aqueous fluid inclusions.

Table 2. Trace element concentration for limestone (NG) and calcite (Cc) samples from the Yax-1 drill core (all concentration in mg/g). For sample origin, see Table 1.

Sample	1801-Cc	1803-Cc	1830-Cc	1836-Cc	1839-Cc	1801-NG	1803-NG	1819-NG	1819-NG-Qz	1830-NG	1836-NG
Rb	<0.02	<0.02	<0.02	<0.02	<0.3	<0.2	<0.2	<0.02	<0.3	0.89	<0.02
Sr	111	179	305	108	144	30.0	145	130	28.0	1118	141
Y	15.1	13.0	2.38	3.19	15.3	0.81	2.38	1.86	0.43	5.98	12.4
Zr	BW	BW	BW	BW	BW	BW	BW	BW	BW	BW	BW
Cs	<0.01	<0.01	<0.01	<0.01	<0.02	<0.02	<0.01	<0.01	<0.02	0.059	<0.01
Ba	0.28	0.39	0.43	1.33	6.40	7.44	4.59	1.23	21.9	222	1.01
La	21.3	13.6	2.22	4.17	48.9	0.61	3.09	1.75	0.39	5.08	12.3
Ce	24.3	11.7	0.87	4.15	80.4	0.74	3.26	2.87	0.66	3.36	14.8
Pr	2.24	0.83	0.24	0.37	6.10	0.07	0.27	0.29	0.04	1.02	1.39
Nd	8.34	3.09	1.00	1.35	22.1	0.28	1.03	1.19	0.20	4.43	5.09
Sm	1.40	0.55	0.18	0.22	3.41	<0.08	0.18	0.22	<0.09	0.92	0.93
Eu	0.33	0.16	0.04	0.06	0.74	<0.02	0.04	0.04	<0.02	0.23	0.22
Gd	1.80	0.99	0.24	0.35	3.31	0.06	0.26	0.19	<0.05	0.95	1.24
Tb	0.24	0.14	0.03	0.04	0.40	<0.01	0.03	0.03	<0.02	0.14	0.18
Dy	1.52	1.03	0.20	0.28	2.09	0.06	0.24	0.17	<0.05	0.83	1.14
Ho	0.34	0.25	0.05	0.06	0.42	0.02	0.05	0.04	<0.02	0.17	0.27
Er	1.00	0.83	0.15	0.18	1.19	0.06	0.18	0.14	<0.05	0.48	0.77
Tm	0.12	0.10	0.02	0.02	0.16	<0.009	0.02	0.02	<0.01	0.05	0.09
Yb	0.71	0.56	0.14	0.12	1.16	<0.05	0.13	0.13	<0.06	0.40	0.53
Lu	0.11	0.09	0.02	0.02	0.19	<0.007	0.02	0.02	<0.09	0.05	0.08
Hf	<0.05	<0.05	<0.05	<0.05	<0.07	<0.06	<0.06	<0.05	<0.07	0.08	<0.05
Pb	1.25	11.0	0.87	6.28	1.13	27.3	16.2	7.88	9.03	2.50	26.4
Th	<0.005	<0.005	<0.005	0.006	<0.008	0.04	0.04	0.37	0.07	0.47	0.01
U	<0.01	0.03	0.55	0.05	<0.02	1.51	2.62	3.90	1.03	3.98	0.44

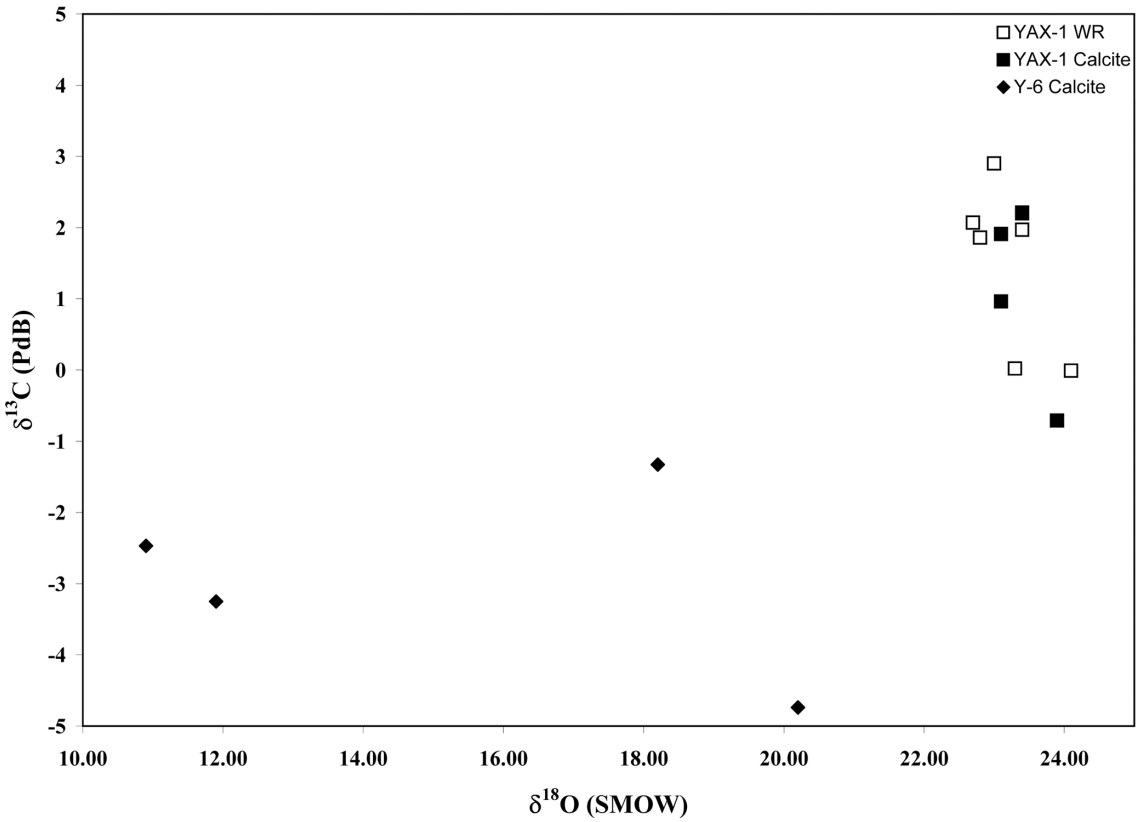

Fig. 3. Carbon and oxygen isotope compositions of calcites and limestone host rocks from the Yax-1 drill core (for sample origin, see Table 1). For comparison, the carbon and oxygen isotope composition of four calcite samples from the drill core Y-6 are shown (data taken from Kettrup et al. 2000). Assuming a homogeneous calcite-forming fluid the lower $\delta^{18}O$ values of the calcites from the Y-6 drill core reflect higher formation temperatures (for details, see text).

Microthermometry, Synchrotron X-Ray Analyses, and Raman Spectroscopy of Fluid Inclusions

Monophase aqueous fluid inclusion hosted in anhydrite were too small to observe any phase transitions during freezing runs.

The ice melting temperatures of rare primary two-phase fluid inclusions in sparry carbonates (calcite, dolomite) and calcite crystals from vugs are highly variable due to melting of ice in the absence of a vapor bubble in most of the studied inclusions. However, melting in the presence of a vapor bubble was observed for some primary inclusions hosted in recrystallized dolomite at 1348.36 m (Fig. 4a and b). The final ice melting temperatures of these inclusions yield salinity between 7.5 and 7.9 wt% NaCl equivalent (Table 1). The salinity of the dolomite-forming fluid was, therefore, considerably higher than the salinity of seawater (~3.2 wt% NaCl equivalent), thus, indicating that circulating seawater heated by the heat-flow of the impact was not the primary source of the mineral-forming fluid. This finding is also strongly confirmed by REE distribution in limestone and calcite (see above).

During heating runs, most of the calcite-hosted fluid inclusions leaked. In smaller inclusions, the homogenization temperatures are reproducible and lie in the temperature range between 65 and 111 °C. The lower homogenization temperatures were always measured in clear calcite, while the higher homogenization temperatures were measured in older, milky calcite or dolomite, respectively. There is no correlation between homogenization temperatures and depth in the drillhole (Table 1). Homogenization temperatures of primary fluid inclusions in calcite do not confirm estimated formation temperatures of about 300 °C based on $\delta^{13}C$ and $\delta^{18}O$ relationships in vein calcites (Zürcher et al. 2003).

Primary type 1 (L+V) inclusions in quartz show salinity in the range between 14–20 wt% equivalent NaCl and homogenization temperatures between 220 and 285 °C. The salinity of halite daughter crystal-bearing type 2 (L+V+S) inclusions lies between 32 and 37 wt% equivalent NaCl as derived from the halite dissolution temperatures (Sterner et al. 1988). Melting of ice was not observed in type 2 inclusions because the liquid did not freeze even when cooling down to temperatures as low as −180 °C. Homogenization temperatures of the vapor bubbles obtained from some type 2 inclusions are always above the halite dissolution temperatures. The latter temperatures can be used to approximate the salinity of type 2 inclusions within a few percent (Chou 1987).

Synchrotron analysis of type 1 and 2 inclusions confirm unusualy high concentrations of metals such as V, Fe, Ni, Cu, Zn, Cd, Sb, Pb contained in the trapped brine (Table 3). High concentrations of V and other metals contained in some of the analyzed fluid inclusions can be explained either by alteration of organic matter by high-salinity fluids at elevated temperatures or by deeply circulating fluids that altered (mafic) basement rocks. Another possible source for metals may be impactites that were hydrothermally altered by saline fluids.

Laser Raman spectroscopy confirmed the presence of hydrocarbons (most probably ethane and propane) in type 3 inclusions. However, it is noteworthy that most of type 3 inclusions highly fluoresce under the Raman laser. Fluid inclusion data could not be measured in these inclusions due to leakage upon heating. The source of these hydrocarbons is likely Cretaceous organic matter. In highly-saline type 1 and 2 inclusions gases were not detected by laser Raman spectroscopy.

DISCUSSION

Fluid inclusion studies in quartz and calcite hosted by Cretaceous sediments of the ICDP-Chicxulub drill core Yax-1 reveal that fluid circulation through the sedimentary rocks was not homogeneous in time and space.

Microthermometric data of quartz-hosted fluid inclusions from fractures about 100 m below the suevitic breccia yield compelling evidence for high-temperature (up to about 285 °C) fluid circulation that was induced by a thermal event,

Table 3. Major and trace element compositions in fluid inclusions in quartz (concentrations in ppm). Sample numbers refer to Table 1.

Sample	1824	1824	1824	1824	1819	1824
Ca	>20000	>20000	>20000	>20000	n.d.	>20000
V	7386	7940	2655	n.d.	n.d.	n.d.
Mn	494	871	n.d.	n.d.	n.d.	25
Fe	16208	24935	826	70	n.d.	174
Ni	638	967	3837	88	243	241
Cu	1767	2502	1727	13	70	44
Zn	2406	15455	>20000	n.d.	99	69
Br	37	218	n.d.	463	1631	257
Sr	99	263	n.d.	372	2024	785
Zr	75	133	n.d.	n.d.	n.d.	n.d.
Nb	9	17	n.d.	n.d	n.d.	n.d.
Cd	169	3323	3910	29	9	14

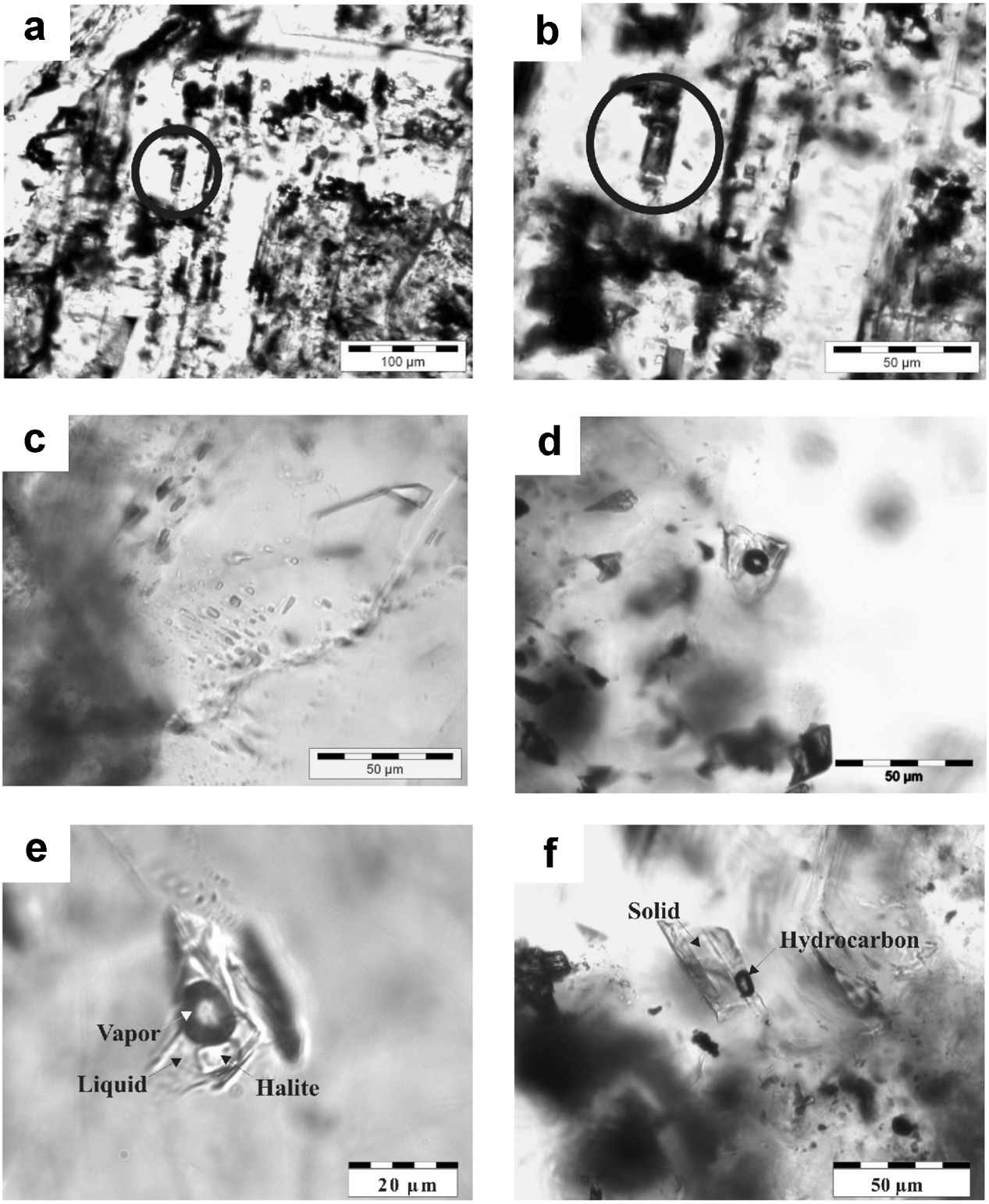

Fig. 4. Microphotographs of a dolomite rhombohedron (a), fluid inclusions in dolomite (a), clear calcite (c), and quartz (d–f) samples from the Yax-1 drill core: a) recrystallized dolomite rhombohedron in limestone (Yax-1_1348.58 m); b) enlargement of (a) showing a primary two-phase fluid inclusions decoration a growth zone of the dolomite rhombohedron; c) trails of aqueous secondary fluid inclusions in younger clear calcite (Yax-1_897.05 m); d) primary two-phase type 1 fluid inclusion in quartz (Yax-1_1000.53 m); e) primary halite daughter crystal-bearing type 2 fluid inclusion in quartz (Yax-1_990.3 m); f) primary hydrocarbon-bearing type 3 fluid inclusion in decorating a growth zone in quartz (Yax-1_1000.53 m).

most probably an impact. The salinities derived from the ice melting temperatures of type 1 (liquid + vapor) inclusions and halite dissolution temperatures of type 2 (L+V+S) inclusions are comparable with fluid inclusion data of anhydrites from the drill hole Y-6 (Gonzales-Partida et al. 2000). The high salinities recorded in fluid inclusions in quartz from the drill core Yax-1 confirm the interpretation of Gonzales-Partida et al. (2000) that the thermal interaction between the meteorite and seawater may have led to the evaporation of seawater or even boiling. However, it is noteworthy, that at a later stage, formation waters were also involved in a mineralizing process, i.e., the precipitation of calcite.

The Yax-1 drill hole is located some 60 km from the center of the impact structure. Thus, it is very unlikely that the whole megablock unit was heated to temperatures of about 300 °C as is inferred from quartz-hosted fluid inclusions. It seems more plausible that, due to the release of large amounts of thermal energy from the meteoritic impact, a large-scale conductive heat-flow was induced that triggered local convection of formation water. In the center of the impact structure, deeply circulating formation waters could have been heated and may have undergone seawater evaporation or even sub-critical two-phase separation (Bischoff and Rosenbauer 1984; Bischoff and Pitzner 1985). Locally, brines formed by such processes could have ascended through fractures in the direction of the crater rim and precipitated quartz on fissures within the Cretaceous sediments. It cannot be excluded that the extreme salinity and the presence of halite daughter crystals in type 2 inclusions resulted from subsurface-near boiling of ascending, hot NaCl-H_2O brines in an open low pressure regime (Fournier 1983). Taking into account that the quartz fractures are hosted in the upper part of the Cretaceous units, the pressure at the time of quartz crystallization would not have exceeded 50 MPa under a hydrostatic pressure regime (considering a sedimentary cover of 200 m and a water depth of 300 m). Hydrothermal fluids as hot as 300 °C may have intersected the boiling curve of the system H_2O-NaCl (Bischoff and Rosenbauer 1984; Bischoff and Pitzner 1985). Trapping of halite daughter crystal-bearing inclusions by boiling is also favored by Gonzales-Partida et al. (2000) for analogue L+V+S inclusions in anhydrite from the drill hole Y-6. Hydrocarbon-bearing (type 3) inclusions were trapped along with type 1 and type 2 inclusions probably due to fluid immiscibility. An intriguing possibility is that the hydrocarbons trapped in type 3 inclusions were derived from the cracking of organic matter. The alteration of organic matter may also be the source of high concentrations of metals such as V, Fe, Ni, Cu, Zn, Cd, Sb, Pb in highly saline fluid inclusions but it can also not be excluded that metals were derived by alteration of impactites or mafic basement rocks. However, the migration of hydrocarbons seems to have occurred at an early stage of hydrothermal activity because fluid inclusions in calcites that precipitated at a later stage (Fig. 1) do not bear hydrocarbons, and the $\delta^{13}C$ values of younger calcites do not reveal evidence for intensive interaction of organic matter with the calcite-forming fluids. This may be indicative for a long-term thermal activity induced by the impact. Preliminary results of the composition of biomarkers in the saturate and aromatic hydrocarbon fractions gave mixed maturity signals but point to a vitrinite reflectance equivalent of 0.8%, which is indicative of formation temperatures in the source rock of between ~100–120 °C (Heroux et al. 1979; Barker and Pawlewicz 1994). Therefore, the hydrocarbons trapped in fluid inclusions in quartz must have originated from cracked organic matter in sediments located closer to the center of the crater rather than from units of the Yax-1 drill core, thus indicating large-scale fluid migration and alteration. While no definitive statement can be made at this stage as to how much of the bitumen is of indigenous or migrated in the studied Yax-1 samples, at least 40% of the organic matter consists of insoluble kerogens and, therefore, had to have present in the analyzed sediments at the time of the meteoritic impact.

It cannot be excluded that (significant?) amounts of hydrocarbons were released to the atmosphere due to impact-induced cracking of organic material. Pope et al. (1997) have calculated the climatic effects of volatiles being released to the stratosphere by the impact and proposed that the greenhouse warming effect caused by impact-generated CO_2 was not significant. However, if hydrocarbons were added to the atmosphere by the Chicxulub event, this would have had a much larger effect on global climate compared to carbon dioxide. At the moment, no statement be can made whether the release of hydrocarbons led to any significant changes of the ancient atmosphere.

Secondary, sparry calcite within the suevitic breccia as well as calcite from vugs hosted by Cretaceous limestone precipitated at considerable lower temperatures than the vug quartz. REE distributions (Fig. 2) and $\delta^{18}O$ versus $\delta^{13}C$ relationships between recrystallized calcite and limestone (Fig. 3) indicate that calcite precipitation occurred from formation waters or fluids that interacted close to the exchange equilibrium with the limestone host rocks before crystallization/mobilization. Most of the homogenization temperatures of fluid inclusions in calcite fell into the temperature range between 75 and 100 °C, thus, indicating that the fluids were heated to about 100 °C. This approximate temperature can also be derived from vitrinite reflectance formation temperatures of organic matter. Since no evidence for significant erosion of Tertiary sediments exists (Pope et al. 1996), a temperature of 100 °C could not have been achieved in a sedimentary pile of 1500 m by burial diagenesis considering a normal thermal gradient of 30 °C/km. It seems very likely that at the Chicxulub site an enhanced thermal gradient was caused by an impact-related conductive heat-flow. Ivanov and Deutsch (1999) have calculated that hydrothermal systems induced by the largest terrestrial

impacts could have been active for up to 2 Ma. In the case of the Chicxulub impact, we conclude that a similar long-term fluid circulation and/or fluid movement through the surrounding rocks was involved. The fluids involved in this process were either heated formation waters or entrained seawater that interacted close to equilibrium with the host rocks. At the Yax-1 drill site, i.e., at the crater rim, the sediments of the megablock were heated homogeneously to about 100 °C probably due to a long-term conductive flow. However, local fluxes of hot, hydrocarbon-bearing brines from convection cell(s) closer to the center of the crater structure seem to have penetrated along faults to the more distant crater rim as well, shortly after the impact. These brines contained hydrocarbons derived from the cracking of organic matter, as documented by (type 3) fluid inclusions trapped in quartz from the Yax-1 drill core.

Acknowledgments–We are indebted to B. Mingram and P. Dulski (both GFZ Potsdam) for the measurements of stable isotopes and trace elements. We are most grateful to T. Kenkmann (HU Berlin) for introducing us to the fascination of impact structures and fruitful discussions. This paper benefited significantly from reviews by Doreen E. Ames and Robert J. Bodnar. The UNAM has provided logistical support during sampling of Yax-1 drill core at Mexico City. The study received financial support from the Deutsche Forschungs Gemeinschaft (DFG) Bonn.

Editorial Handling—Dr. Dieter Stöffler

REFERENCES

Alvarez L. W., Alvarez W., Asaro F., and Michel H. V. 1980. Extraterrestrial cause for the Cretaceous-Tertiary mass extension. *Science* 208:1095–1108.

Ames D. E, Watkinson D. H., and Parrish R. R. 1998. Dating of a regional hydrothermal system induced by the 1850 Ma Sudbury impact event. *Geology* 26:447–450.

Barker E. B. and Pawlewicz M. J. 1994. Calculation of vitrinite reflectance from thermal histories and peak temperatures: A Comparison of methods. In *Vitrinite reflectance as a maturity parameter—Applications and limitations,* edited by Dow W. G. American Chemical Society Symposium Series 570:216–229.

Bau M. and Möller P. 1992. Rare earth element fractionation in metamorphic hydrothermal calcite, magnesite and siderite. *Mineralogy and Petrology* 45:231–246.

Bau M. and Dulski P. 1996. Distribution of yttrium and rare-earth elements in the Penge and Kuruman Iron Formations, Transvaal Supergroup, South Africa. *Precambrian Research* 79:37–55.

Bischoff J. F. and Pitzner K. S. 1985. Phase relations and adiabats in boiling seafloor geothermal systems. *Earth and Planetary Science Letters* 75:327–338.

Bischoff J. F. and Rosenbauer R. J. 1984. The critical point and two-phase boundary of seawater, 200–500 °C. *Earth and Planetary Science Letters* 68:172–180.

Boer R. H., Reimold W. U., Koeberl C., and Kesler S. E. 1996. Fluid inclusion studies on drill core samples from the Manson impact crater: Evidence for post-impact hydrothermal activity. Special Paper 302. Boulder: Geological Society of America. pp. 377–382.

Chou I. M. 1987. Phase relations in the system NaCl-KCl-H_2O. III. Solubilities of halite in vapor-saturated liquids above 445 °C and redetermination of phase equilibrium properties in the system NaCl-H_2O to 1000 °C and 1500 bars. *Geochimica et Cosmochimica Acta* 51:1965–1975.

Clayton R. N., O'Neil J. R., and Mayeda T. K. 1972. Oxygen isotope exchange between water and quartz. *Journal of Geophysical Research* 77:3057–3067.

Crossey L. J., Kudo A. M., and McCarville P. 1994. Post-impact hydrothermal systems: Manson impact structure, Manson, Iowa (abstract). 25th Lunar and Planetary Science Conference. pp. 299–300.

Dence M. R., Grieve R. A. F., and Robertson P. B. 1977. Terrestrial impact structures: Principal characteristics and energy considerations. In *Impact and explosion cratering,* edited by Roddy D. J., Pepin R. O., and Merill R. B. Oxford: Pergamon Press. pp. 247–275.

Dressler B. O., Sharpton V. L., Morgan J., Buffler R., Moran D., Smit J., Stöffler D., and Urrutia J. 2003. Investigating a 65-Ma-old smoking gun: Deep drilling of the Chicxulub impact structure. *Eos Transactions* 84:130.

Dulski P. 2001. Reference materials for geochemical studies: New analytical data by ICP-MS and critical discussion of reference values. *Geostandards and Geoanalysis* 25:87–125.

Fournier R. O. 1983. Active hydrothermal systems as analogues of fossil systems. Special Report 13. Geothermal Resources Council. pp. 263–284.

Gonzales-Partida E., Charillo-Chavez A., and Martinez-Ibarra R. 2000. Fluid inclusions from anhydrite related to the Chicxulub crater impact breccias, Yucatán, Mexico: Preliminary Report. *International Geological Review* 42:279–288.

Gurov E. P., Koeberl C., and Reimold W. U. 1998. Petrography and geochemistry of target rocks and impactites from the Ilyinets crater, Ukraine. *Meteoritics & Planetary Science* 33:1317–1333.

Hecht L., Schmitt R. T., and Wittmann A. 2003. Hydrothermal alteration of the impactites at the ICDP drill site Yax-1 (Chicxulub crater) (abstract #1583). 34th Lunar and Planetary Science Conference. CD-ROM.

Heroux Y., Chagnon A., and Bertrand R. 1979. Compilation and correlation of major thermal maturation indicators. *Bulletin of the American Association of Petroleum Geologists* 12:2128–2144.

Hildebrand A. R., Penefield G. T., Kring D. A., Pilkington A., Camargo-Zanoguera R., Jacobson S., and Boynton W. V. 1991. Chicxulub crater: A possible Cretaceous/Tertiary boundary impact crater on the Yucatán Penninsula. *Geology* 19:867–871.

Ivanov B. and Deutsch A. 1999. Sudbury impact event: Cratering mechanics and thermal history. In *Large meteorite impacts and planetary evolution II,* edited by Dressler B. O. and Sharpton V. L. Special Paper 339. Boulder: Geological Society of America. pp. 389–397.

Kenkmann T., Wittmann A., Scherler D., and Schmitt R. T. 2003. Deformation features of the Cretaceous units of the ICDP-Chicxulub drill core Yax-1 (abstract #1368). 34th Lunar and Planetary Science Conference. CD-ROM.

Kettrup B., Deutsch A., Ostermann M., and Agrinier P. 2000. Chicxulub impactites: Geochemical clues to the precursor rocks. *Meteoritics & Planetary Science* 35:1229–1238.

Kirsimae K., Suuroja S., Kirs J., Kärki A., Polikarpus M., Puura V., and Suuroja K. 2002. Hornblende alteration and fluid inclusions in Kärdla impact crater, Estonia: Evidence for impact-induced hydrothermal activity. *Meteoritics & Planetary Science* 37:449–457.

Koeberl C., Fredricksson K., Götzinger M., and Reimold W. U. 1989. Anomalous quartz from the Roter Kamm impact crater, Namibia:

Evidence for post-impact hydrothermal activity? *Geochimica et Cosmochimica Acta* 53:2113–2118.

Komor S. C., Valley J. W., and Brown P. E. 1988. Fluid inclusion evidence for impact heating at the Siljan Ring, Sweden. *Geology* 16:711–715.

Krogh T. E., Kamo S. L., Sherton V. L., Marin L. E., and Hildebrand A. R. 1993. U-Pb ages of single shocked zircons linking distal K/T impact ejecta to the Chicxulub crater. *Nature* 366:731–734.

Lechtenberg F., Garbe S., Bauch J., Dingwell D. B., Freitag F., Haller M., Hansteen T. H., Ippach P., Knöchel A., Radtke M., Romano C., Sachs P. M., Schmincke H. U., Ullrich H. J. 1996. The X-ray fluorescence measurement place at beamline L of HASYLAB. *Journal of Trace and Microprobe Techniques* 14:561–587.

Lüders V., Horsfield B., Kenkmann T., Mingram B., and Wittmann A. 2003. Hydrocarbons and aqueous fluids in Cretaceous sediments of the ICDP-Chicxulub drill core Yax-1 (abstract #1378). 34th Lunar and Planetary Science Conference. CD-ROM.

Möller P., Rosenthal E., Dulski P, Geyer S., and Guttman Y. 2003. Rare earths and yttrium hydrostratigraphy along the Lake Kinneret-Dead Sea-Arava transform fault, Israel and adjoining territories. *Applied Geochemistry* 18:1613–1628.

Molnar F., Watkinson D. H., and Everest J. O. 1999. Fluid-inclusion characteristics of hydrothermal Cu-Ni-PGE veins in granitic and metavolcanic rocks at the contact of the Little Stobie deposit, Sudbury, Canada. *Chemical Geology* 154:279–301.

Molnar F., Watkinson D. H., and Jones P. C. 2001. Multiple hydrothermal processes in footwall units of the North Range, Sudbury Igneous Complex, Canada, and implications for the genesis of vein-type Cu-Ni-PGE deposits. *Economic Geology* 96:1645–1670.

Morgan J. V., Warner M. R., Collins G. S., Melosh H. J., and Christeson G. L. 2000. Peak-ring formation in large impact craters: Geophysical constraints from Chicxulub. *Earth and Planetary Science Letters* 183:347–354.

O'Neil J. R., Clayton R. N., and Mayeda T. K. 1969. Oxygen isotope fractionation in divalent metal carbonates. *Journal of Chemical Physics* 51:5547–5558.

Osinski G. R., Spray J. G., and Lee P. 2001. Impact-induced hydrothermal activity within the Haughton impact structure, arctic Canada: Generation of a transient, warm, wet oasis. *Meteoritics & Planetary Science* 36:731–745.

Pope K. O., Ocampo A. C., and Duller C. E. 1991. Mexican site for K/T impact crater? *Nature* 351:105–106.

Pope K. O., Ocampo A. C., Kinsland G. L., and Smith R. 1996. Surface expression of the Chicxulub crater. *Geology* 24:527–530.

Pope K. O., Baines K. H., Ocampo A. C., and Ivanov B. A. 1997. Energy, volatile production, and climatic effects of the Chicxulub Cretaceous/Tertiary impact. *Journal of Geophysical Research* 102:21645–21664.

Rickers K., Thomas R., and Heinrich W. 2004. Trace-element analysis of individual synthetic and natural fluid inclusions with synchrotron radiation XRF using Monte Carlo simulations for quantification. *European Journal of Mineralogy* 16:23–35.

Roedder E. 1984. Fluid inclusions. *Reviews of Mineralogy* 12:1–644.

Sterner S. M., Hall D. L., and Bodnar R. J. 1988. Synthetic fluid inclusions. V. Solubility relations in the system NaCl-KCl-H_2O under vapor-saturated conditions. *Geochimica et Cosmochimica Acta* 52:989–1006.

Stöffler D., Ewald U., Ostertag R., and Reimold W. U. 1977. Research drilling Nördlingen 1973 (Ries): Composition and texture of polymict impact breccias. *Geologica Bavarica* 75: 163–185.

Sturkell E. F. F. 1998. The marine Lockne impact structure, Jamtland, Sweden: A review. *Geologische Rundschau* 87:253–267.

Sturkell E. F. F., Broman C., Forsberg P., and Torssander P. 1998. Impact-related hydrothermal activity in the Lockne impact structure, Jamtland, Sweden. *European Journal of Mineralogy* 10:589–606.

Van Espen P., Janssens K., and Swenters I. 1992. AXIL X-ray analysis software. Manual and Computer Program. Belgium: University of Antwerp.

Veizer J. 1992. Depositional and diagenetic history of limestones: Stable and radiogeneic isotopes. In *Isotopic signatures and sedimentary records,* edited by Clauer N. and Chaudhuri S. New York: Springer Verlag. pp. 13–48.

Vincze L., Janssens K., and Adams F. 1993. A general Monte Carlo simulation of energy-dispersive X-ray fluorescence spectrometers—Part I. *Spectrochimica Acta* 48:553–573.

Vincze L., Janssens K., Adams F., and Rindby A. 1995a. A detailed ray-tracing code for capillary X-ray optics. *X-Ray Spectrometry* 24:27–37.

Vincze L., Janssens K, Adams F, Rivers M. L., and Jones K. W. 1995b. A general Monte Carlo simulation of energy-dispersive X-ray fluorescence spectrometers—Part II. *Spectrochimica Acta* 50:127–148.

Vincze L., Janssens K., Adams F., and Jones K. W. 1995c. A general Monte-Carlo simulation of energy dispersive X-ray fluorescence spectrometers—Part III. *Spectrochimica Acta* 50:1481–1500.

Webb G. E. and Kamber B. S. 2002. Rare earth elements in Holocene reefal microbialites: A new shallow seawater proxy. *Geochimica et Cosmochimica Acta* 64:1557–1565.

Zheng Y. F. 1994. Oxygen isotope fractionation in metal monoxides. *Mineralogical Magazine* 58:1000–1001.

Zürcher L., Kring D. A., Dettmann D., and Rollog M. 2003. Stable isotope record of post-impact fluid activity in the Chicxulub crater as exposed by the Yaxopoil-1 borehole (abstract #1728). 34th Lunar and Planetary Science Conference. CD-ROM.